A COMPUTATIONAL ANALYSIS OF OPERATIONAL PARAMETERS INFLUENCING COAL GASIFICATION IN A LAB-SCALE DROP TUBE GASIFIER

Sunel KUMAR [1], Zhihua WANG[2,3], Shuang WANG *[1], Yaw Dwamena-AKENTENG[1], Ding JIANG[1], Hao CHEN[1]

[1] School of Energy and Power Engineering, Jiangsu University, Jiangsu 212013, China

[2]Qingshanhu Energy Research Center, Zhejiang University, 311300, Hangzhou, P. R. China

[3]State Key Laboratory of Clean Energy Utilization, Zhejiang University, 310027, Hangzhou, China

[*] Corresponding author; E-mail: alexjuven@ujs.edu.cn

This study uses a numerical simulation for coal gasification operation in a drop tube gasifier to investigate the effects of wall temperature and oxygen-to-coal (O/C) ratios on gasification. Coal gasification is an efficient approach to electricity generation, offering a cleaner alternative to conventional coal combustion methods. A 2D Computational Fluid Dynamics (CFD) model of the gasifier was employed to perform grid sensitivity analysis and subsequently compute the influences of varying wall temperatures (1000 K, 1250 K, and 1500 K) and O/C ratios (0.6, 0.8, 1, and 1.2) on the temperature profile, syngas composition, and velocity within the gasifier. Temperature profiling within the furnace defined a spectrum of maximum and minimum temperatures, with apex values recorded at 2100 K and lowest values at 1300 K for Cases 12 and 1, respectively. High O/C ratios favored the production of CO_2 due to enhanced combustion reactions, whereas lower O/C ratios were conducive to higher yields of CO and H_2, essential syngas components. Velocity profiles of particles within the gasifier increased with higher temperatures and O/C ratios, and the maximum velocity was 9 m/sec. In conclusion, this study offers valuable insights into optimizing operational parameters such as wall temperatures and O/C ratios to enhance the performance and efficiency of coal gasification processes in lab-scale gasifiers.

Keywords*: Coal Gasification; Oxygen-to-Coal Ratio (O/C Ratio); Computational Fluid Dynamics (CFD); Reaction Kinetics; Syngas Composition*

1. Introduction

Coal gasification is a process that converts coal into a versatile gas called syngas, which can be used to generate electricity and manufacture a range of chemical products. This approach taps into coal's potential more efficiently [1]. The escalating electricity demand has historically been met predominantly by oil. However, there has been a noticeable shift towards exploring coal usage in recent research due to depleting oil reserves and the prevalent availability of coal in China [2]. Gasification technology has emerged as a potential avenue for maximizing energy conversion into

electricity with minimal hazardous impacts. Researchers' main aim is to develop sophisticated gasifiers that exhibit enhanced performance and reduced emissions of pollutants [3-6]. Studies have been conducted to understand the chemical and physical changes occurring during the gasification process to optimize the transformation of coal into gas. Alongside experimental analyses, Computational Fluid Dynamics (CFD) simulations offer a cost-efficient method to examine factors such as reaction rates, temperature variations, turbulent intensity, the proportions of oxygen and coal, and coal retention time, among others. Nevertheless, CFD modeling of gasification necessitates distinctive mathematical models to analyze and decipher the complexities associated with turbulence, temperature variations, and reaction rates to yield meaningful outcomes.

Numerous researchers have recently undertaken several studies involving CFD simulations in entrained flow coal gasifiers [7-14]. Mukyeong et al. [15] used steam as a gasifying agent, evaluated the performance of the IGCC coal gasifier, and also revealed that tangential inflow influences the particle motion. A study by Shaohua et al. [16] on the simulation of mixing coal with PET in co-gasification within a fluidized bed discovered that larger particle sizes impede heat flow. Kim et al. [17] ran a simulation and found that for coal gasification in a 300 MW IGCC, an oxygen/coal ratio of 0.7 is ideal. Diba et al. [18] found that the optimum airflow for char conversion was 17 kg/h and that calcination resulted in a higher concentration of carbon dioxide. Sun et al. [19] investigate the impact of immersed tubes on gas-particle interactions in fluidization dynamics using CFD simulation, which plays a crucial role in the efficiency and efficacy of biomass gasification. Dmitry et al. [20] developed an enhanced analytical model to predict heat transfer in entrained-flow gasifiers. This model specifically accounts for the flow and heat transfer characteristics of the slug layer wall in the reactor during dry-feed coal gasification.

Researchers have experimented with mixed gasification agents with syngas, attaining temperatures of more than 1550°C through a numerical approach [21]. Wang et al. [22] employed discrete-phase and solidification models to perform computational simulations to recover heat from molten slugs and syngas. Euler-Euler [23, 24] and Euler-Lagrangian methods [9, 25-27] have also been applied by researchers to delineate gas and solid flows. Commonly, FR/ED and probability density functions (PDF) have been employed to analyze the chemistry of gasification reactions, with various mediums like air/steam being used for gasification [28-30]. Watanabe et al. [31] studied the modeling and simulation of coal gasification in an entrained flow coal gasifier, reviewed the three chemical processes, and discussed the accuracy of the model. In diverse CFD simulations, parameters like gasification reactions, nozzle design, and particle size have been explored [12, 32-36]. A study by Imran et al. [37] examines the gasification process for multi-injectors at different O/C ratios, revealing hydrogen composition up to 28% and CO at 52%, indicating that pure oxygen leads to elevated temperatures and enhanced carbon conversion efficiencies.

In our research, a 2D drop tube gasifier is analyzed, initially focusing on grid sensitivity analysis, followed by an assessment of wall temperature effects at 1000, 1250, and 1500K with various O_2/coal ratios (0.6, 0.8, 1, 1.2). This approach allows the computation of temperature profiles, syngas compositions, and velocity profiles. The gasification process has been successfully modeled, showing that finite rates significantly influence global chemical reactions.

2. Simulation Model

2.1. Gasifier mesh and design

Figure 1 displays the 2D gasifier drawing; the gasifier operates as a downflow reactor and consists of two parts, with a throat between them, with a height of 3.83 meters. The inner diameters of the first and second stages are 0.250 meters each. Two levels of injection are incorporated into the gasifier. The upper level has three coal inlets and two oxygen inlets, as illustrated in Figure 1. Conversely, the lower level contains two opposing coal injections. The gasifier operates at a total dry coal feeding rate of 50 kg/h, with the lower inlet featuring a surface-type injection situated at 1.910 meters. Detailed proximate and ultimate analyses of the coal are presented in Table 1. Particle size corresponds to the Rosin-Rammler method, with the maximum, minimum, and mean diameters of 0.125 mm, 0.004 mm, and 0.0456 mm, respectively. In the upper stage, pulverized coal undergoes an exothermic reaction with oxygen, resulting in a temperature increase through the devolatilization of coal into char and carbon dioxide. Following this, the second injection stage leverages the generated heat to facilitate an endothermic reaction, primarily yielding carbon monoxide and hydrogen, with a minor carbon dioxide production. Calculations for the required oxygen can be based on the Oxygen/Coal ratio of the fixed carbon feeding. While the oxygen injection remains constant at the upper level, coal distribution is evenly split, with 50% at the upper and 50% at the lower.

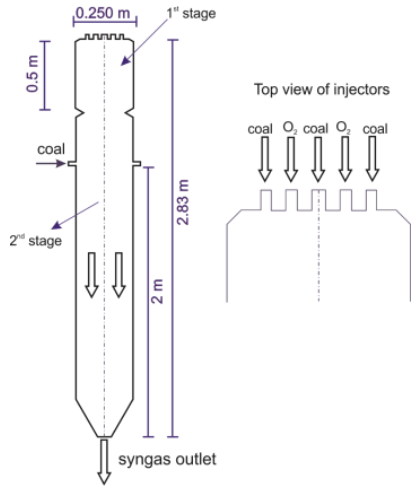

Figure 1 Illustrating the Drop Tube Gasifier furnace

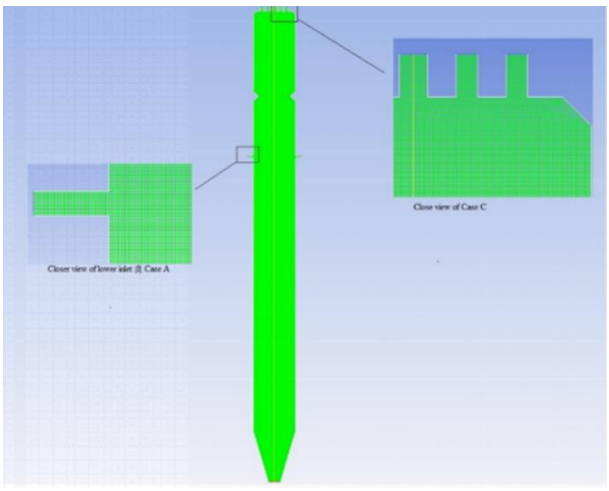

Figure 2 The detailed representation of the 2D meshed geometry illustrates a zoomed-in view of the upper inlets (right) and the lower inlet (left).

Table 1 Ultimate and proximate analyses of coal.

Proximate (% ad)				$Q_{net,\ ad}$ (J/g)	Ultimate (% ad)				
Ash (A)	Moisture (M)	Fix carbon (FC)	Volatile (V)		Hydrogen (H)	Carbon (C)	Oxygen (O)	Sulfur (S)	Nitrogen (N)
10.30	13.84	47.09	28.77	24,237	3.27	62.03	9.49	0.37	0.70

Note: $Q_{net,\ ad}$ is the term used for Lower Heating Value, M denotes Moisture Content, FC stands for Fixed Carbon, ad refers to Air-Dry Basis, A signifies Ash Content, V represents Volatile Content.

2.2. Governing equation

The numerical analysis in this study involves a two-dimensional structure and considers both homogeneous and heterogeneous reactions operating under steady and incompressible turbulence conditions. Consequently, species, time-averaged steady-state pressure-based Navier-Stokes, mass momentum, and energy equations have been resolved. The equations that govern the numerical simulation are provided in the following manner [13]:

$$\frac{\partial}{\partial x_i}(\rho u_{ij}) = S_m \tag{1}$$

$$\frac{\partial}{\partial x_i}(\rho c_p u_i T) = \frac{\partial}{\partial x_i}\left(\lambda \frac{\partial T}{\partial x_i} - \rho c_p \overline{u_i' T'}\right) + \mu\Phi + S_h \tag{2}$$

$$\frac{\partial}{\partial x_i}(\rho u_i u_j) = \rho \bar{g}_j - \frac{\partial P}{\partial x_i} + \frac{\partial}{\partial x_i}(\tau_{ij} - \rho \overline{u_i' u_j'}) + S_j \tag{3}$$

$$\frac{\partial}{\partial x_i}(\rho u_i C_j) = \frac{\partial}{\partial x_i}\left(\rho D_i \frac{\partial C_j}{\partial x_i} - \rho \overline{u_i' C_j'}\right) + S_j \tag{4}$$

The Reynolds stress is denoted by $\rho \overline{u_i' u_j'}$, and symmetric stress tensor is τ_{ij}. The equation governing turbulent flow was resolved by employing realizable *k-ε*, and the kinematic turbulence viscosity was calculated based on equation (5). The dissipation rate is denoted as ε, while ƙ symbolizes the turbulence kinetic energy and the. viscosity constant is represented as C_μ. These values can be determined using the subsequent standards ƙ-ε transport equations: [38]

$$\mu_t = \rho C_\mu k^2/\varepsilon \tag{5}$$

$$\frac{\partial}{\partial x_i}(\rho u_i k) = \frac{\partial}{\partial x_i}[(\mu + \frac{\mu_t}{\sigma_k})\frac{\partial k}{\partial x_i}] + G_k - \rho\varepsilon \tag{6}$$

$$\frac{\partial}{\partial x_i}(\rho u_i \varepsilon) = \frac{\partial}{\partial x_i}[(\mu + \frac{\mu_t}{\sigma_\varepsilon})\frac{\partial \varepsilon}{\partial x_i}] + C_{1\varepsilon} G_k \frac{\varepsilon}{k} + C_{2\varepsilon} G_k \frac{\varepsilon^2}{k} \tag{7}$$

In the provided model, the turbulence kinetic energy represents the $G_ƙ$ resulting from the mean velocity gradients. The turbulent Prandtl numbers related to the turbulent kinetic energy (ƙ) and its

dissipation rate (ε) are symbolically represented by σ_k and σ_ε, respectively. Constants such as $C_{1\varepsilon}$ equals 1.44, C_μ equals 0.009, σ_k equals 1.0, $C_{2\varepsilon}$ equals 1.92, and σ_ε equals 1.3 in Launder and Spalding's work [39] were utilized in equations (6-7). Additionally, turbulence heat conductivity (λ) and the diffusion coefficient (D) were specified in the equation. (3-4):

$$\rho C_p \overline{u_i' T'} = -\lambda \frac{\partial T}{\partial x_i} = C_p \frac{\mu_t}{\mathrm{Pr}_t} \frac{\partial T}{\partial x_i} \tag{8}$$

$$\rho \overline{u_i' C_j} = -\rho D_i \frac{\partial C_j}{\partial x_i} = -\frac{\mu_t}{Sc_t} \frac{\partial C_j}{\partial x_i} \tag{9}$$

Sc_t (=0.7) and Pr_t (=0.85) denote the Schmidt numbers and turbulence Prandtl. The Discrete Phase Model (DPM) was employed to determine particles' momentum using the Lagrangian method. In the Lagrangian reference frame context, the combined balance force acting on the coal was used to approximate the trajectory of discrete phase particles. This balanced force evaluates the coal's inertia against forces acting as substitutes for the coal, as presented in reference [40].

$$\frac{du_p}{dt} = F_D(u - u_p) + g_x \frac{\rho_p - \rho}{\rho_p} + F_x \tag{10}$$

The formulated equations account for the reduction in particle mass and thermal energy by incorporating source terms that facilitate the exchange between the continuous and discrete phases. The P-1 equation is responsible for determining the interaction of radiation between gas and various particles. Within the P-1 equation, the model mentioned [63] is used to ascertain the radiation intensity.

$$-\nabla q_r = aG - 4aG\sigma T^4 \tag{11}$$

Where

$$q_r = -\frac{1}{3(a + \sigma_s) - C\sigma_s} \nabla G \tag{12}$$

The symbols G, σ, a, C, and σs stand for incident radiation, Stefan-Boltzmann constant, absorption coefficient, linear anisotropic phase function coefficient, and scattering coefficient, respectively.

2.3. Gasification primary reaction

Equation (4), the equation for species transport, is useful for identifying key kinetic characteristics and examining the chemical processes inside a gasifier. Nonetheless, because of the intense heat within the gasifier, the coal is converted into char, volatile compounds, and ash [41]. The composition released from the coal is illustrated in the subsequent equation (13) [42]. In the zone of intense heat where coal particles are exposed to high temperatures, the introduction of coal from above sets off a series of chemical and physical variations [34]. These initial processes contain the

gasification of char, the burning of any residual char and volatile substances, and the devolatilization of coal. All volatile substances identified in our research were grouped under one category, represented by the formula $C_{1.45}H_{4.64}O_{0.44}$. This categorization was based on the elemental composition of the coal, as revealed in Table 1. To describe how volatile substances are released, we used a model that breaks down the process into two distinct stages [43] to characterize the release of volatiles, as detailed below:

$$\text{Coal} \rightarrow \alpha_1 \text{ volatiles} + \alpha_2 \, H_2O + \alpha_3 \text{ char} + \alpha_4 \text{ Ash} \tag{13}$$

$$Coal \xrightarrow{k_l} (1 - Y_l) \times Char_l + Y_l \times Volatile \tag{14}$$

$$Coal \xrightarrow{k_h} (1 - Y_h) \times Char_h + Y_h \times Volatile \tag{15}$$

In the equation, Y denotes the stoichiometric coefficient. The lower temperature is depicted in equation (14), while the 15th equation indicates a faster reaction rate at elevated temperatures. The expression of the kinetic reaction is as follows:

$$\frac{dV}{dt} = (k_l Y_1 + k_h Y_h) Coal \tag{16}$$

$$k_h = A_h \exp(-E_h / RT_p) \tag{17}$$

$$k_l = A_l \exp(-E_l / RT_p) \tag{18}$$

The volatile mass fraction is denoted by the symbol V, the letter k denotes the pre-exponential factor, the rate constant of the reaction is denoted by the letter k, the temperature of the coal particle is denoted by the symbol TP, and the reaction activation energy is denoted by the symbol E. Data related to values of k_l, Y_l, kh, Yh, Eh, and E_l were extrapolated from prior research [39, 40], and are tabulated in [44]. The coal devolatilization culminates in the formation of char, which subsequently undergoes gasification to produce CO and H_2. Researchers have employed many reactions to characterize the gasification processes [9, 13, 14, 23, 25-27, 45]. In the present study, various initial reactions were examined to determine the most effective reaction mechanism. Relevant instances are listed in [44].

The heterogeneous reactions were characterized by multiple volatile chemical species involved in the reaction mechanisms, namely H_2O, CO, $C_{(s)}$, O_2, N_2, CO_2, and H_2. A species transport model was meticulously selected, incorporating particle surface interactions, volumetric reactions, and turbulence-chemistry interactions. These aspects were quantitatively delineated by utilizing the FR/ED model. This computational model facilitated the precise determination of the formation rates of the individual species, allowing for the contemporary updating source term, Sr, as given in Equation (4).

$$S_r = M_j \sum_{j=1}^{N} w_{j,r} \tag{19}$$

$$w_{j,r} = \left(v''_{j,r} - v'_{j,r}\right) k_f \left(\prod_{i=1}^{N_r} [C]^{\eta''} - \frac{1}{K_{eq}} \prod_{i=1}^{N_r} [C]^{\eta''} \right) \quad (20)$$

$$k_f = AT^B e^{(-E_a/RT)} \quad (21)$$

Under the principles of the Arrhenius equation, several parameters such as kf, *B*, *Ea*, and A have been delineated to characterize the kinetics of the forward reaction. Here, kf represents the rate constant of the forward reaction, *B* denotes the temperature exponent, *Ea* symbolizes the activation energy requisite for the reaction to proceed, and *A* represents the pre-exponential factor or frequency of collision. References from previous studies [13, 36, 46] have been utilized to ascertain the values of Ea, *A*, and *B* pertinent to various reactions, which have subsequently been cataloged and presented in [44] for comprehensive analysis and reference.

2.4. Simulation method

Table 1 presents the composition of the coal used. The coal feed rate was maintained at 50 kilograms per hour across various studies, each employing distinct oxygen-to-coal ratios. The boundary conditions were mass flow inlets and pressure outlets used for all input/output stream. A fixed wall exhibiting a no-slip condition (meaning that the fluid has zero velocity at the boundary) with a consistent roughness value of 0.5 was modeled. The Discrete Phase Model (DPM) wall interaction was set to a reflective type for both normal and tangential particle impacts using a polynomial relationship. This setup was examined under different wall temperature conditions: 1500 K, 1250 K, and 1000 K. Temperature plays a key role in the gasification process, making it a primary focus of our grid sensitivity study. Three different densities of mesh have been selected for analysis of temperature and velocity. Figure 2 presents the meshed domain, including a closer view of the nozzles. Furthermore, the initial reaction was determined at various oxygen/coal ratios like 0.60, 0.80, 1, and 1.20 at different wall temperatures like 1000 K, 1250 K, and 1500 K, as shown in Table 2.

The compositional details of the coal utilized in the experiment are defined in Table 1. A consistent coal feeding rate of 50 kg/h was maintained across all case studies, each characterized by varying O_2/coal ratios. Boundary conditions were established for all input and output streams, incorporating mass flow inlets and pressure outlets. The walls were considered stationary with a no-slip condition (zero velocity) applied, maintaining a constant roughness of 0.5. Regarding the Discrete Phase Model (DPM), the walls were designated as reflective, implementing a polynomial type for both normal and tangent interactions. Wall temperatures were manipulated, applying 1500 K, 1250 K, and 1000 K values to assess their influences. Given its critical influence on gasification processes, temperature was prioritized as a key parameter within the grid sensitivity analysis. A selection of mesh densities, varying across three distinct categories, was applied to facilitate a comprehensive analysis of temperature and velocity parameters. Refer to Figure 2 for a detailed visualization of the meshed domain, including a magnified view featuring the nozzles' structural intricacies. Initiating reactions were strategically selected, incorporating varied oxygen/coal ratios such as 0.60, 0.80, 1, and 1.20. These ratios were meticulously paired with diverse wall temperatures, specifically 1000 K, 1250 K, and 1500 K, as systematically categorized in Table 2.

Table 2 Different scenarios simulated for a range of oxygen-to-coal ratios and wall temperatures.

Case	1	2	3	4	5	6	7	8	9	10	11	12
O/C	0.6	0.6	0.6	0.8	0.8	0.8	1	1	1	1.2	1.2	1.2
Temp:	1000	1250	1500	1000	1250	1500	1000	1250	1500	1000	1250	1500

3. Results and Discussion

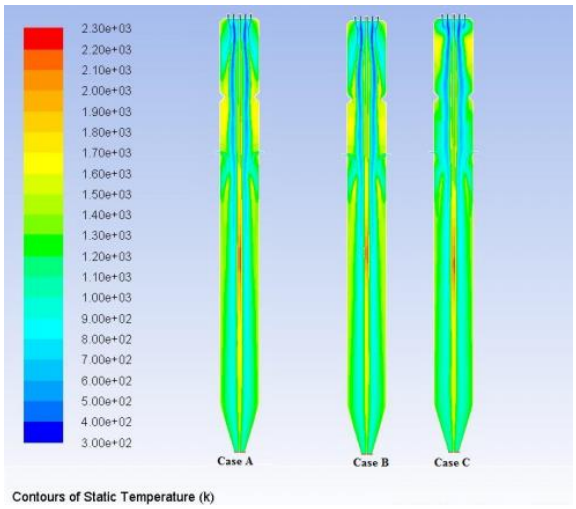

Figure 3 Temperature (K) distribution for grid sensitivity analysis (three grid sizes).

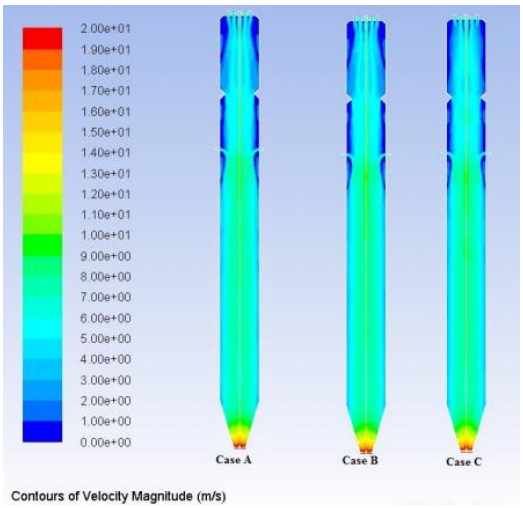

Figure 4 Velocity (m/s) profile for grid sensitivity analysis.

3.1. Evaluation of Model Validation Through Grid Sensitivity Analysis

In the gasification processes, temperature is the paramount parameter influencing outcomes. Consequently, scenarios (Cases A, B, and C) were meticulously chosen for grid sensitivity analysis to scrutinize the variations and impacts associated with temperature fluctuations. Figure 2 illustrates the meshed domain, accompanied by a detailed view of the nozzles. Non-reactive cold flow simulations were conducted using three distinct grid configurations. The subsequent temperature profiles, aligned with the velocity vectors across these grids, are comprehensively shown in Figures 3 and 4, respectively. The grids for cases A, B, and C are 529,091, 339,027, and 236,855, respectively; the grid consists of structured and unstructured mesh. The tetrahedral cells demonstrate a uniform temperature distribution along the central axis, vertical to the height of the gasifier. The velocity profile is almost the same along with height, but minor changes are observed near the top of the gasifier. However, the overall result shows that grid sensitivity does not influence temperature and velocity profile. The solution demonstrates grid independence for grid sizes exceeding 339,027. Consequently, this specific grid size has been adopted for subsequent computations.

3.2. Impact of the oxygen-to-coal (O/C) Ratio and Wall Temperature on Synthesis Gas Generation

Several critical parameters predominantly influence the performance of an oxygen-blown drop tube furnace. The oxygen concentration, temperature, and the oxygen-to-coal (O/C) ratio play pivotal roles in determining the operational efficacy of the gasifier. These variables substantially influence the furnace's behavior and overall gasification effectiveness. The combustion reaction influences the generation of CO_2 species, the thermal output requisite for endothermic reactions, and the subsequent formation of CO and H_2. A series of twelve simulation cases were meticulously analyzed, varying in Oxygen-to-coal (O/C) ratios (0.6, 0.8, 1, and 1.2) and temperatures (1000, 1250, and 1500 K), as detailed in Table 2. Figure 5 illustrates how changes in the oxygen-to-carbon (O/C) ratios and temperature levels affect the composition of syngas. Specifically, Figure 5 (a) shows the variance in CO composition across different temperatures and O/C ratios, emphasizing a heightened mass fraction of CO composition in the gasifier's upper regions. Contrarily, it was discerned that wall temperature exerted minimal influence on the composition. Figure 5 (b) shows that the CO_2 composition at the injection site was comparatively reduced. However, a subsequent series of reactions evidenced an amplification in CO_2 formation, with elevated O/C ratios particularly conducive to this increase. A general trend was identified where an ascent in the O/C ratio culminated in an enhanced CO_2 percentage, attributed predominantly to the water-gas shift reaction. Conversely, an elevation in temperature resulted in a diminished CO_2 percentage, substantiated.

Figure 5 (c) illustrates an obvious variation in the hydrogen mass fraction under different operational parameters. At an O/C (oxygen-to-coal) ratio of 0.6, a substantial hydrogen mass fraction is observed predominantly in the upper region. This propensity, however, diminishes when coal is introduced through the second injection point, leading to a reduced hydrogen fraction. A comparative analysis between different cases (1-6 versus 8-12) reveals a conspicuous disparity in the hydrogen fraction. Cases 1-6 exhibit a more elevated hydrogen fraction than cases 8-12, implying that a higher O/C ratio may not be conducive to optimal hydrogen production. In addition, the investigation elucidates that temperature variations exhibit a nominal influence on the yield of H_2. The findings suggest that the reaction's efficiency was compromised due to a shortage of steam, which is essential

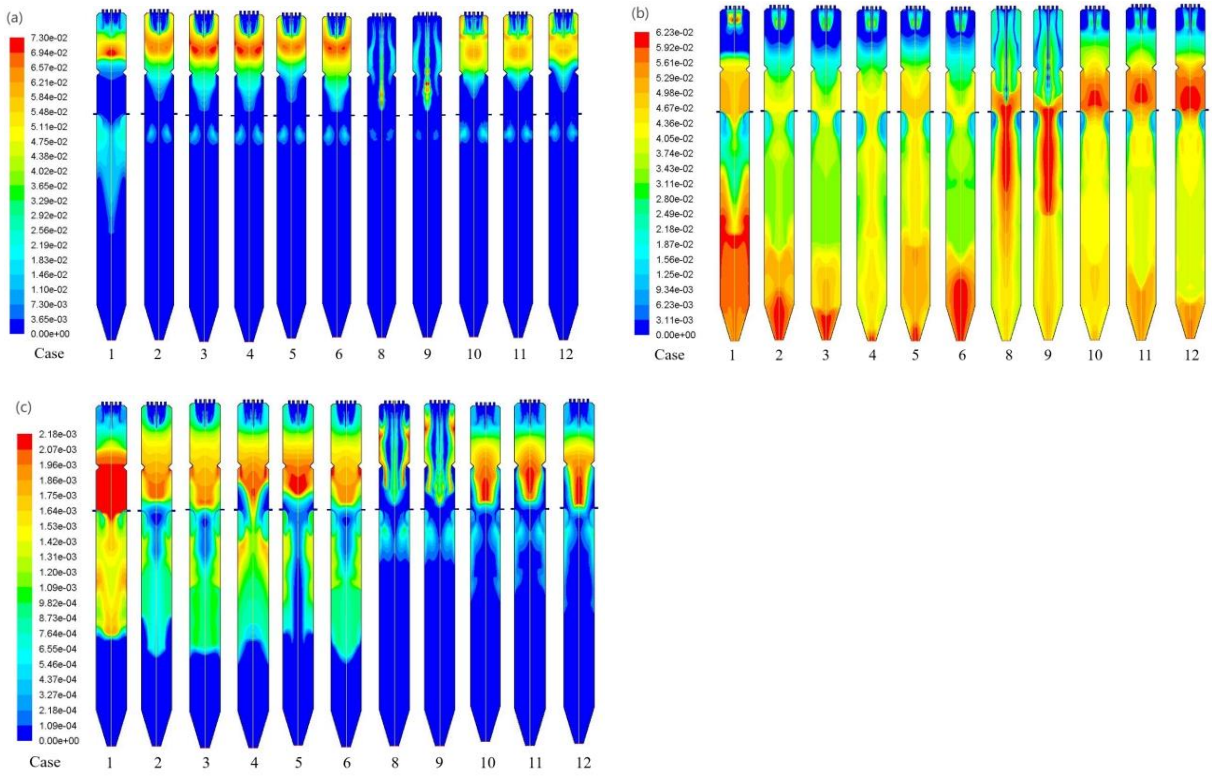

Figure 5 Influence of wall temperature and O/C ratios on coal gas composition (a) CO mass fraction, (b) CO_2 mass fraction, (c) H_2 mass fraction.

for the water-gas shift reaction to proceed. This was because the simulations took place in an environment with plenty of oxygen but without steam.

3.3. Impact of O/C Ratio and Temperature on the Temperature profile

In the gasification/combustion reaction, the temperature parameter emerged as a pivotal variable. Increasing the amount of oxygen led to a higher temperature in the top part of the gasifier. A delineation of the temperature profile within the furnace is exhibited in Figure 6, elucidating a conspicuous augmentation in temperature concurrent with increments in the wall temperature and oxygen-to-coal (O/C) ratio. Extreme temperature values were considered 2100 K and 1300 K for Cases 12 and 1, respectively. A relatively lower temperature gradient characterizes the thermal profile within the upper section of the gasifier. This is attributed to the injection of 50% of the coal feed at this upper injection point, coupled with the spatial limitation due to the upper region's reduced height

compared to the gasifier's lower region. Consequently, the lower region manifests a heightened temperature profile due to its extended vertical dimension. Factors such as an elevated oxygen-to-coal (O/C) ratio and increased wall temperatures significantly enhance the gasifier's thermal conditions.

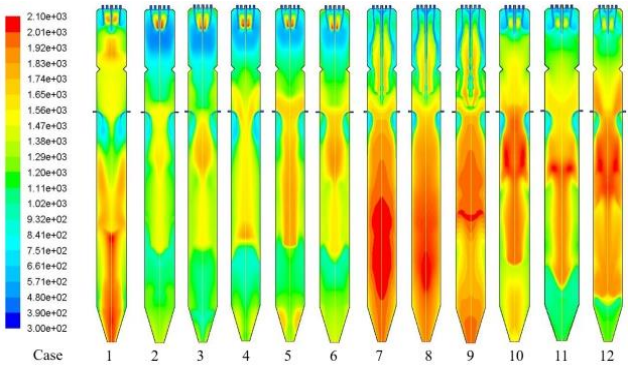

Figure 6: Variation in syngas temperature (K) under different operating conditions of the gasifier.

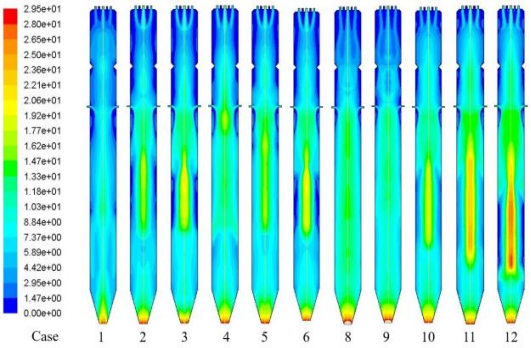

Figure 7 Velocity profile for drop tube gasifier.

3.4. Velocity profile for drop tube furnace

Figure 7 depicts the velocity profiles for cases 1 through 12. It can be discerned from the data that a direct correlation exists between the particle's velocity, the prevailing temperature, and the O/C ratio. The peak velocity registered was 9 m/sec, and interestingly, an inverse relationship between the height of the gasifier and the velocity was observed. Due to gravitational force, coal particles drop down without external forces. However, lower injections are side injections that the lower velocity at the inner wall of the gasifier may cause. However, the curve shape between the two also causes the particle to have low velocity. However, the curve shape also helps to increase the velocity of the lower injection particle, which is why the velocity at the lower region of the gasifier is high.

4. Conclusion

This comprehensive study investigates a 2D Computational Fluid Dynamics (CFD) model of a drop tube gasifier, focusing on grid sensitivity and the effects of varying wall temperatures (1000 K to 1500 K) and O_2/coal ratios (0.6 to 1.2) on gasifier performance. The study finds that the gasifier's efficiency is significantly influenced by oxygen concentration, temperature, and the oxygen-to-coal (O/C) ratio. Notably, the mass fraction of carbon monoxide (CO) is higher in the furnace's upper regions, while carbon dioxide (CO_2) concentration is minimal near the injection zones. Wall temperature appears to have a limited impact on CO composition.

A key observation is the interaction between temperature, O/C ratio, and CO_2 composition. An increase in O/C ratio leads to higher CO_2 levels due to the water-gas shift reaction, whereas higher temperatures decrease CO_2 percentages. Hydrogen fraction analysis shows an optimized presence at an O/C ratio of 0.6, mainly in the upper furnace regions. A decrease in hydrogen fraction is noted with secondary coal injections. Comparative studies between different cases suggest variations in hydrogen presence linked to O/C ratios.

Temperature profiling within the furnace reveals a range of maximum (2100 K) and minimum (1300 K) temperatures, with lower gradients in the upper regions due to operational dynamics. In contrast, the lower regions exhibit higher temperature profiles. Velocity profiling indicates a correlation with

temperature and O/C ratios, with a notable increase in particle velocities at higher temperatures and O/C ratios, reaching a maximum of 9 m/sec. This study highlights the complex dependencies of operational parameters on the gasifier's performance, providing valuable insights for optimizing gasification processes.

Acknowledgment

This work was supported by the Fundamental Research Funds for the Central Universities (2021FZZX001-11) and the National Natural Science Foundation of China (52125605).

Nomenclature

E_a	activation energy for reaction (J/K mol)
A	pre-exponential factor (consistent units)
B	temperature constant (dimensionless)
η'	rate exponent for product reactant species
η''	rate exponent for product species
k_f	forward reaction rate constant
ρ, ρ_p	density, density of particles (kg/m^3)
u, u_p	velocity, velocity of particles (m/s)
c_p	specific heat at constant pressure (J/kg K)
C_j	mole fraction of species j
C_μ	viscosity constant
$[C]$	molar concentration of species (K mol/m^3)
C	coefficient of function for linear-anisotropic phase
τ_{ij}	symmetric stress tensor
σ	Stefan–Boltzmann constant
σ_s	scattering coefficient (m^{-1})
$v'_{i,r}$	Stoichiometric coefficient for reactant i in reaction r
$v''_{j,r}$	Stoichiometric coefficient for product j in reaction r
D_i	diffusivity (m^2/s)
D_t	diffusion coefficient for turbulence (m^2/s)
S_m, S_j, S_h, S_r	source terms for mass, momentum, energy and Species
T	temperature (K)
λ	turbulent thermal conductivity (W/m K)
M_j	molecular weight of specie j
Wj,r	Net production rate of species i through chemical reaction (K mol/m^{3}S)
$\mathcal{E}_W$	emissivity
α	absorption coefficient
G	incident radiation

q_r	heat flux for radiation heat ($J/m^2 s$)
S_{c_t}	Schmidt number for turbulence
P_{r_t}	Prandtl number for turbulence
G_k	mean velocity gradients
μ_t	turbulence viscosity
ε	dissipation rate of turbulence (m^2/s^3)
k	kinetic energy for turbulence (m^2/s^2)
μ	dynamic viscosity ($N S/m^2$)
F_D	drag force (kg m/s)

References

[1] Yamauchi Y, Akiyama K. Innovative Zero-emission Coal Gasification Power Generation Project. Enrgy Proced. 2013;37:6579-86.
[2] Wang Q, Li R. Journey to burning half of global coal: Trajectory and drivers of China′s coal use. Renewable and Sustainable Energy Reviews. 2016;58:341-6.
[3] Taniguchi M, Yamamoto K, Kobayashi H, Kiyama K. A reduced NOx reaction model for pulverized coal combustion under fuel-rich conditions. Fuel. 2002;81:363-71.
[4] Taniguchi M, Kamikawa Y, Okazaki T, Yamamoto K, Orita H. A role of hydrocarbon reaction for NOx formation and reduction in fuel-rich pulverized coal combustion. Combustion and Flame. 2010;157:1456-66.
[5] Molina A, Murphy JJ, Winter F, Haynes BS, Blevins LG, Shaddix CR. Pathways for conversion of char nitrogen to nitric oxide during pulverized coal combustion. Combustion and Flame. 2009;156:574-87.
[6] Ampah JD, Jin C, Agyekum EB, Afrane S, Geng Z, Adun H, et al. Performance analysis and socio-enviro-economic feasibility study of a new hybrid energy system-based decarbonization approach for coal mine sites. Science of The Total Environment. 2023;854:158820.
[7] Xu S, Ren Y, Wang B, Xu Y, Chen L, Wang X, et al. Development of a novel 2-stage entrained flow coal dry powder gasifier. Applied Energy. 2014;113:318-23.
[8] Qin S, Chang S, Yao Q. Modeling, thermodynamic and techno-economic analysis of coal-to-liquids process with different entrained flow coal gasifiers. Applied Energy. 2018;229:413-32.
[9] Fletcher DF, Haynes BS, Christo FC, Joseph SD. A CFD based combustion model of an entrained flow biomass gasifier. Applied Mathematical Modelling. 2000;24:165-82.
[10] Gharebaghi M, Irons RM, Pourkashanian M, Williams A. An investigation into a carbon burnout kinetic model for oxy–coal combustion. Fuel Processing Technology. 2011;92:2455-64.
[11] Jeong HJ, Seo DK, Hwang J. CFD modeling for coal size effect on coal gasification in a two-stage commercial entrained-bed gasifier with an improved char gasification model. Applied Energy. 2014;123:29-36.
[12] Slezak A, Kuhlman JM, Shadle LJ, Spenik J, Shi S. CFD simulation of entrained-flow coal gasification: Coal particle density/sizefraction effects. Powder Technology. 2010;203:98-108.
[13] Silaen A, Wang T. Effect of turbulence and devolatilization models on coal gasification simulation in an entrained-flow gasifier. International Journal of Heat and Mass Transfer. 2010;53:2074-91.
[14] Gerun L, Paraschiv M, Vîjeu R, Bellettre J, Tazerout M, Gøbel B, et al. Numerical investigation of the partial oxidation in a two-stage downdraft gasifier. Fuel. 2008;87:1383-93.
[15] Kim M, Sohn G, Ye I, Ryu C, Kim B, Lee J. Numerical analysis on the performance of a 300 MW IGCC coal gasifier under various operating conditions. Fuel. 2019;257:116063.
[16] Du SH, Yuan SZ, Zhou Q. Numerical investigation of co-gasification of coal and PET in a fluidized bed reactor. Renew Energ. 2021;172:424-39.
[17] Kim M, Sohn G, Ye I, Ryu C, Kim B, Lee J. Numerical analysis on the performance of a 300 MW IGCC coal gasifier under various operating conditions. Fuel. 2019;257.
[18] Diba MF, Karim MR, Naser J. CFD modelling of coal gasification in a fluidized bed with the effects of calcination under different operating conditions. Energy. 2022;239.

[19] Sun H, Bao G, Yang S, Hu J, Wang H. Numerical investigation on the influence of immersed tube bundles on biomass gasification in industrial-scale dual fluidized bed gasifier. Fuel. 2024;357:129742.
[20] Safronov D, Förster T, Schwitalla D, Nikrityuk P, Guhl S, Richter A, et al. Numerical study on entrained-flow gasification performance using combined slag model and experimental characterization of slag properties. Fuel Processing Technology. 2017;161:62-75.
[21] Fang N, Lu Y, Li ZQ, Lu Y, Chen ZC. Improving mixing and gasification characteristics in an industrial-scale entrained flow gasifier with a novel burner. J Clean Prod. 2022;362.
[22] Wang B, Qiu JY, Guo QH, Gong Y, Xu JL, Yu GS. Numerical Simulations of Solidification Characteristics of Molten Slag Droplets in Radiant Syngas Coolers for Entrained-Flow Coal Gasification. Acs Omega. 2021;6:20388-97.
[23] Vicente W, Ochoa S, Aguillón J, Barrios E. An Eulerian model for the simulation of an entrained flow coal gasifier. Appl Therm Eng. 2003;23:1993-2008.
[24] Álvarez L, Gharebaghi M, Jones JM, Pourkashanian M, Williams A, Riaza J, et al. Numerical investigation of NO emissions from an entrained flow reactor under oxy-coal conditions. Fuel Processing Technology. 2012;93:53-64.
[25] Choi YC, Li XY, Park TJ, Kim JH, Lee JG. Numerical study on the coal gasification characteristics in an entrained flow coal gasifier. Fuel. 2001;80:2193-201.
[26] Watanabe H, Otaka M. Numerical simulation of coal gasification in entrained flow coal gasifier. Fuel. 2006;85:1935-43.
[27] Ajilkumar A, Sundararajan T, Shet USP. Numerical modeling of a steam-assisted tubular coal gasifier. International Journal of Thermal Sciences. 2009;48:308-21.
[28] Huynh CV, Kong S-C. Performance characteristics of a pilot-scale biomass gasifier using oxygen-enriched air and steam. Fuel. 2013;103:987-96.
[29] Hongtao L, Feng C, Xia P, Kai Y, Shuqin L. Method of oxygen-enriched two-stage underground coal gasification. Mining Science and Technology (China). 2011;21:191-6.
[30] Silva VB, Rouboa A. Using a two-stage equilibrium model to simulate oxygen air enriched gasification of pine biomass residues. Fuel Processing Technology. 2013;109:111-7.
[31] Watanabe H, Kurose R. Modeling and simulation of coal gasification on an entrained flow coal gasifier. Advanced Powder Technology. 2020;31:2733-41.
[32] Kong X, Zhong W, Du W, Qian F. Compartment modeling of coal gasification in an entrained flow gasifier: A study on the influence of operating conditions. Energy Conversion and Management. 2014;82:202-11.
[33] Seo H-K, Park S, Lee J, Kim M, Chung S-W, Chung J-H, et al. Effects of operating factors in the coal gasification reaction. Korean Journal of Chemical Engineering. 2011;28:1851.
[34] Du S-W, Chen W-H, Lucas J. Performances of pulverized coal injection in blowpipe and tuyere at various operational conditions. Energy Conversion and Management. 2007;48:2069-76.
[35] Singer S, Chen L, Ghoniem AF. The influence of gasification reactions on char consumption under oxy-combustion conditions: Effects of particle trajectory and conversion. Proceedings of the Combustion Institute. 2013;34:3471-8.
[36] Chen C-J, Hung C-I, Chen W-H. Numerical investigation on performance of coal gasification under various injection patterns in an entrained flow gasifier. Applied Energy. 2012;100:218-28.
[37] Unar IN, Wang LJ, Pathan AG, Mahar RB, Li RD, Uqaili MA. Numerical simulations for the coal/oxidant distribution effects between two-stages for multi opposite burners (MOB) gasifier. Energ Convers Manage. 2014;86:670-82.
[38] Jones WP, Launder BE. The prediction of laminarization with a two-equation model of turbulence. International Journal of Heat and Mass Transfer. 1972;15:301-14.
[39] Launder BE, Spalding DB. The numerical computation of turbulent flows. Computer Methods in Applied Mechanics and Engineering. 1974;3:269-89.
[40] Gonzalo-Tirado C, Jiménez S, Ballester J. Gasification of a pulverized sub-bituminous coal in CO2 at atmospheric pressure in an entrained flow reactor. Combustion and Flame. 2012;159:385-95.
[41] Chen W-H, Du S-W, Yang T-H. Volatile release and particle formation characteristics of injected pulverized coal in blast furnaces. Energy Conversion and Management. 2007;48:2025-33.
[42] Wen CY, Chaung TZ. Entrainment coal gasification modeling. I & EC - Industrial and Engineering Chemistry1979. p. 684-95.
[43] Wang L, Jia Y, Kumar S, Li R, Mahar RB, Ali M, et al. Numerical analysis on the influential factors of coal gasification performance in two-stage entrained flow gasifier. Applied Thermal Engineering. 2017;112:1601-11.

[44] Kumar S, Wang Z, He Y, Zhu Y, Cen K. Numerical Analysis for Coal Gasification Performance in a Lab-Scale Gasifier: Effects of the Wall Temperature and Oxygen/Coal Ratio. Energies. 2022;15:8645.
[45] Chui EH, Majeski AJ, Lu DY, Hughes R, Gao H, McCalden DJ, et al. Simulation of entrained flow coal gasification. Energy Procedia. 2009;1:503-9.
[46] Ubhayakar SK, Stickler DB, Von Rosenberg CW, Gannon RE. Rapid devolatilization of pulverized coal in hot combustion gases. Symposium (International) on Combustion. 1977;16:427-36.

Submitted: 22.11.2023
Revised: 11.01.2024
Accepted: 23.01.2024